MIT Open Access Articles

Mapping thixo-elasto-visco-plastic behavior

Citation: Ewoldt, Randy H., and Gareth H. McKinley. "Mapping Thixo-Elasto-Visco-Plastic Behavior." Rheologica Acta 56, no. 3 (March 2017): 195–210.

As Published: http://dx.doi.org/10.1007/s00397-017-1001-8

Publisher: Springer Berlin Heidelberg

Persistent URL: http://hdl.handle.net/1721.1/107482

Version: Author's final manuscript: final author's manuscript post peer review, without publisher's formatting or copy editing

Massachusetts Institute of Technology

Mapping Thixo-Visco-Elasto-Plastic Behavior

Randy H. Ewoldt

Department of Mechanical Science and Engineering,

University of Illinois at Urbana-Champaign, Urbana, IL 61801, USA

Gareth H. McKinley

Department of Mechanical Engineering,

Massachusetts Institute of Technology, Cambridge, MA, USA

Abstract

A century ago, and more than a decade before the term rheology was formally coined, Bingham introduced the concept of plastic flow above a critical stress to describe steady flow curves observed in English china clay dispersion. However, in many complex fluids and soft solids the manifestation of a yield stress is also accompanied by other complex rheological phenomena such as thixotropy and viscoelastic transient responses, both above and below the critical stress. In this perspective article we discuss efforts to map out the different limiting forms of the general rheological response of such materials by considering higher dimensional extensions of the familiar Pipkin map. Based on transient and nonlinear concepts, the maps first help organize the conditions of canonical flow protocols. These conditions can then be normalized with relevant material properties to form dimensionless groups that define a three-dimensional state space to represent the spectrum of Thixotropic Elastoviscoplastic (TEVP) material responses.

*Corresponding authors: ewoldt@illinois.edu, gareth@mit.edu

Introduction

One hundred years ago, Eugene Bingham published his first paper investigating "the laws of plastic flow", and noted that *"the demarcation of viscous flow from plastic flow has not been sharply made"* (Bingham 1916). Many still struggle with unambiguously separating such concepts today, and indeed in many real materials the distinction is not black and white but more grey or gradual in its characteristics. With the explosion of interest in the flow of soft matter systems over the past few decades, and ready access to advanced rheometry systems, our objective here is to describe how to "map" regimes of different rheological complexities, especially for including and demarcating nonlinear, viscoelastic, thixotropic, and plastic behavior.

In the introduction to his original article, Bingham quotes directly and re-emphasizes earlier comments of Maxwell who clearly appreciated the distinctions between "perfectly elastic", "soft or plastic", and "viscous fluid" states. Both Bingham and Maxwell emphasized the need for careful consideration of the relevant time scales and force scales for distinguishing between these different states of matter. Bingham's careful studies of changes in the fluidity (or reciprocal of viscosity) of a series of model English china clays over a wide range of concentrations and temperatures ultimately led to the development of the constitutive model (or rheological equation of state) now known as the Bingham plastic.

The rheological response of many real-world materials of interest (such as highly-filled gels and pastes, foodstuffs and other consumer products) often depends on both the time-scale *and* the level of force imposed, and furthermore also often show a time-varying or thixotropic response even at a fixed amplitude of forcing (e.g. at a controlled stress or controlled deformation rate). The underlying microstructure of such materials typically consists of a high volume fraction of a strongly interacting discrete 'particulate' phase (consisting, for example, of

spheroidal particles, droplets, fibers, platelets or combinations thereof) imbedded in a viscous (or possibly viscoelastic) continuous matrix phase. Reversible deformation of the microstructure by (small) externally imposed deformations can store energy elastically; however as the strain amplitude is increased, microstructural rearrangements on progressively larger length scales lead to irreversible and permanent (or 'plastic') deformation as well as viscous dissipation [(Boromand et al. 2017; Jamali et al. 2017)]. Such materials are therefore best described, in the most general case, as *Thixotropic Elasto-Visco-Plastic* (or TEVP) materials and ongoing challenges are faced in both experimentally measuring the rheological characteristics of such materials as well as approaches to modeling each isolated aspect of the constitutive response as the imposed force or processing time scale is varied (Denn and Bonn 2011).

The goal of this short perspective article is not to review in extensive detail all of the recent contributions made in quantifying each of these independent aspects of the material response. Excellent reviews are available of both viscoplasticity (Balmforth et al. 2013; Bonn et al. 2015) and thixotropic effects (Barnes 1997; Mewis and Wagner 2009) on their own as well as different approaches to constitutive modeling of this behavior (de Souza Mendes and Thompson 2012; Fraggedakis et al. 2016a). Instead we seek to consider holistically how to isolate, understand and describe the interactions of these different rheological phenomena using modern test protocols and instrumentation, and how to represent the relative importance of different thixotropic, elastic, viscous and plastic contributions using suitable maps and design charts.

In recent years the Pipkin diagram, proposed by A. C. Pipkin in his Lectures on Viscoelasticity (Pipkin 1972) has re-established itself as the canonical map for graphically communicating and representing distinctions between linear and nonlinear viscoelastic phenomena (Hyun et al. 2011; Bharadwaj and Ewoldt 2014; Swan et al. 2014; Osswald and

Rudolph 2015; Carter et al. 2016). We extend this foundational paradigm to include thixotropic

phenomena and to locate the Bingham model (see Fig.1 below), and moreover to show how to

map different flow conditions and test protocols to help guide rheological characterization

(Figs.3-6). These maps represent a systematic way of extending the Pipkin diagram to describe

materials that are not just linearly or nonlinearly viscoelastic (VE), but which also have stress-

induced changes and transient responses that occur on different timescales than viscoelastic

relaxation, and which may therefore collectively be referred to as thixotropic in character
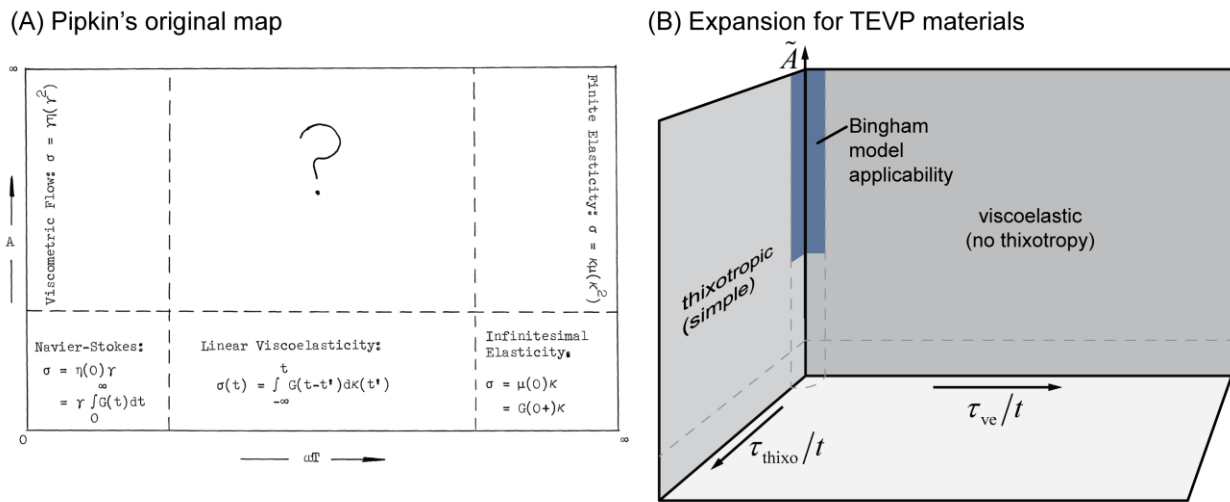
(Barnes 1997).

Figure 1. Merging Bingham and Pipkin to accommodate Thixo-Elasto-Visco-Plastic (TEVP) materials. (A) Pipkin's original map (Pipkin 1972) of nonlinear viscoelasticity (the abscissa is the imposed frequency ω multiplied by characteristic viscoelastic relaxation time T, the ordinate is dimensionless strain amplitude) (reused with permission of Springer). Thixotropy and plasticity were not described. (B) We expand the Pipkin map to account for thixotropic timescales τ_{thixo} when they are conceptually distinct from viscoelastic relaxation timescales τ_{ve}. The timescale t represents the transient timescale of the deformation. Beyond constitutive model mapping (e.g. the Bingham model applicability region is shown for steady plastic flow above a yield stress), this framing can be used to map actual flow and rheological test conditions. As we shall see, we generalize the amplitude $\tilde{A}$ to be either strain, rate-of-strain, or stress; the choice depends on the circumstance, e.g. the criteria for plastic flow, or the naturally controlled amplitude of the deformation.

4

The Pipkin map extended

Transient and *Nonlinear*: these two keywords are foundational to organizing rheological complexity, and were concepts used by Pipkin in his original diagram shown in Figure 1(A). About his map, Pipkin wrote (Pipkin 1972):

> *"Laminar shearing flows can be classified, loosely, by assigning to each flow a characteristic shear amplitude A and a frequency ω. We will interpret these parameters very broadly, but for present purposes, to fix ideas one may think of ordinary sinusoidal shearing of a thin layer of fluid."*

The strain amplitude *A* defines the ordinate (vertical) axis, representing the direction to travel on the map to see nonlinearity. The transient timescale defines the abscissa (horizontal) axis; Pipkin used a dimensionless transient timescale corresponding to frequency ω multiplied by a characteristic viscoelastic relaxation time (which he denoted *T* and which we will generically denote t), a grouping we now identify as the Deborah number, *De*.

With this framing in Figure 1(A), the limit of linear viscoelasticity is at the bottom edge, nominally below the dashed horizontal line at small amplitudes. The limit of steady but nonlinear behavior is along the left edge, for low frequencies or, equivalently, long transient times $t \to \infty$. A Newtonian fluid, which does not incorporate viscoelasticity and rheological nonlinearity, is relegated to the lower left corner of the Pipkin map.

The provocative question mark in the middle of the map corresponds to Pipkin's statement that *"Nothing very systematic is known about the interior region…"* because no systematic constitutive model generally applies to unsteady flows of viscoelastic fluids at large strains. Actually, there is something systematic known about other edges, notably the slightly nonlinear (asymptotically-nonlinear) region just above the linear limit based on the memory integral expansion. This was acknowledged by Pipkin and has been an area of recent interest for

characterization, and is now often known as medium-amplitude oscillatory shear (MAOS) (Davis and Macosko 1978; Giacomin et al. 2011; Wagner et al. 2011; Ewoldt and Bharadwaj 2013; Bharadwaj and Ewoldt 2015). Additionally, the retarded motion expansions (a.k.a. ordered fluid expansions) systematically extend away from the Newtonian fluid along both axes, e.g. as shown recently with a fourth-order fluid expansion (Bharadwaj and Ewoldt 2014). Very recently, the uppermost edge of the Pipkin map has been explored with extra-extra-large amplitude oscillatory shear (XXLAOS) (Ewoldt 2016; Khair 2016a; Khair 2016b), though at present, the exploration is model specific, and not universal. Moreover, most of these "systematic" regions only consider nonlinear *viscoelasticity*, and completely leave out thixotropy.

Pipkin focused on viscoelasticity and did not consider thixotropy. The phrase "thixo" does not appear anywhere in his "Lectures on Viscoelasticity Theory" (Pipkin 1972), and is clearly outside the scope as suggested by the title of the lectures. More generally, however, we might consider transient phenomena to include thixotropic breakdown and buildup, in addition to viscoelastic relaxation and retardation. This requires an additional *transient* axis of the Pipkin space, as shown in Figure 1(B), so that one can compare flow timescales t to thixotropic timescales (denoted generically as τ_{thixo}). We thus can identify a dimensionless ratio of time scales τ_{thixo}/t to parameterize this axis (here we have used the transient timescale t to highlight the general concept rather than a frequency $w \gg 2p/t$ as used by Pipkin). This generic thixotropic evolution in the material might lead to changes in the viscosity of the material and/or the critical stress (i.e. the history dependent yield stress required to support steady flow) in the material, and we discuss both effects in more detail below. Quite generally however, thixotropic effects now correspond to regions offset from the "viscoelastic backplane" that was originally drawn by

Pipkin. In fact, all simple thixotropic fluid models, without viscoelasticity, describe behavior on this separate "thixotropic" plane shown in Figure 1(B).

With this expanded three-dimensional map, we must address the persistent question of what amplitude of forcing to use for the vertical axis (Ewoldt et al. 2012). Although Pipkin used shear strain, a more general treatment must recognize that this amplitude A may be strain, rate-of-strain, or stress (or dimensionless forms thereof); the choice depends on the circumstance, such as the constitutive model or flow process of interest, as we shall illustrate with several examples later. For now, we note that nonlinearities to be expected at large dimensionless amplitudes $\tilde{A} > 1$ would generally include shear-thinning and shear-thickening, normal stress differences, thixotropic breakdown or buildup, and plasticity. If we generalize the map to include *extensional* flow kinematics, and not just shear as considered by Pipkin, then strain hardening would be an additional nonlinear effect to appear at large amplitudes. One can imagine separate Pipkin maps for describing both extensional and shear flow if strongly nonlinear effects are of interest.

The three different possible amplitudes of forcing (strain, strain rate, and stress) can also be expressed in dimensionless form. The strain-rate can be normalized by a timescale to make a Weissenberg number $Wi = \tau_{ve}\dot{\gamma}$ (typically a viscoelastic time scale is used, but thixotropic timescales may be more natural in some cases (Blackwell and Ewoldt 2014)). The Weissenberg number describes fluid nonlinearity, in contrast to the Deborah number which describes viscoelasticity and flow unsteadiness, as nicely articulated by (Dealy 2010).

The strain amplitude g_0 itself is of course already dimensionless, but soft solid materials may yield over a wide range of different strain amplitudes; for example many biopolymer gels and food gums may withstand strains as large as $g_c \gg 1$ (100% strain) before gradually softening and flowing, whilst colloidal and particulate gels may show more pronounced and abrupt transitions

at very small strains as small as $g_c \gg 10^{-2}$ or smaller. Normalizing the imposed value with respect to the critical strain amplitude g_c results in a dimensionless group $G = g_0/g_c$ with much deeper and universal meaning. For the final possibility, the amplitude A could be a stress, e.g. in the case of creep compliance testing or controlled oscillatory shear stress. In this case the appropriate dimensionless stress amplitude should be normalized by a critical stress amplitude (e.g. a yield stress, S_y) to give a dimensionless variable $\Sigma = \sigma_0/\sigma_y$.

When mapping the predictions of constitutive models of complex *fluids*, choosing the (dimensionless) rate-of-strain (Weissenberg number) for the ordinate offers several benefits, primarily the ability to map the ordered fluid expansions, which are perturbations from the Newtonian limit for "slow and slowly-varying flows" (Bird et al. 1987) (i.e. uniformly valid expansions for small Deborah and Weissenberg numbers, respectively). If one is more interested in rheologically complex *solids*, where a Newtonian flow limit is unnecessary, then the strain amplitude (normalized by a critical strain) may be more appropriate. Stress amplitude may be most relevant for yield stress fluids, such as the Bingham model with a critical yield stress.

The critical value of amplitude causing nonlinearity is generally a function of the transient timescale, creating a non-trivial "linear" boundary line. Some very general results have been established by considering small deviations from linear viscoelasticity (Astarita and Jongschaap 1978; Ewoldt and Bharadwaj 2013; Bharadwaj and Ewoldt 2015). Typically, at low Deborah numbers (when fluid behavior dominates) a critical strain *rate* causes nonlinearity, whereas at high Deborah numbers (when elastic solid behavior dominates) a critical *strain* causes the nonlinearity. The shape of the linear limit boundary in terms of critical stress is an open question not yet addressed in the literature.

With the expanded Pipkin map in Figure 1(B), one may now ask, where does the traditional Bingham model fit on the Pipkin space? It is not linear at small amplitude, so it cannot touch the linear regime. It also neglects viscoelastic and thixotropic transients, so it is restricted to the back left corner of Figure 1(B). It does not touch the lower corner of Newtonian behavior, unless the model is regularized to include a linear, Newtonian regime, as in the Papanastasiou regularization (Papanastasiou 1987). Any real flow scenario with transient conditions may not be appropriately modeled by the Bingham model, e.g. sphere sedimentation, depending on the level of accuracy desired in the predictions.

It is worth noting some current uses of the Pipkin map paradigm, to give context to how we will expand the usage. The traditional usage of the Pipkin map is mainly for (i) collecting and organizing regions of applicability for different constitutive models that describe nonlinear viscoelasticity or (ii) showing the results of material characterizations with large-amplitude oscillatory shear (LAOS). Examples of constitutive model mapping include (Dealy and Wissbrun 1990; Macosko 1994; Bharadwaj and Ewoldt 2014; Ewoldt 2014). Examples of mapping LAOS characterization are perhaps even more common, e.g. (Reimers and Dealy 1996; Reimers and Dealy 1998; Ewoldt et al. 2008; Swan et al. 2014; Osswald and Rudolph 2015; Ewoldt 2016; Khair 2016a). The LAOS mapping can appear as surface plots across the Pipkin Space, and we invite the reader to enjoy the particularly forward-thinking visualization of Thurston & Pope (Thurston and Pope 1981) (their Figures 4-5), which include 3D stereoscopic views of LAOS harmonics as a function of amplitude and frequency. Each figure includes a stereoscopic pair of separate images, depicting left-eye and right-eye views of the same response surface. When viewed together, our brains perceive a single three-dimensional surface as a function of the inputs of frequency and amplitude.

We will consider both dimensionless and *dimensional* Pipkin maps, the latter of which is particularly useful for mapping flow conditions in a specific process independent of a particular material's timescales. First though, we consider mapping material properties themselves, independent of the flow conditions. Such figures take the flavor of Ashby-style cross-property plots (Ashby 1999); providing the timescales and properties needed to make dimensionless Pipkin maps.

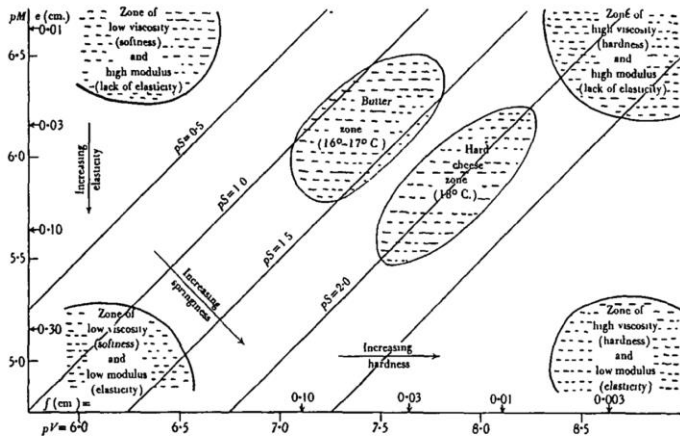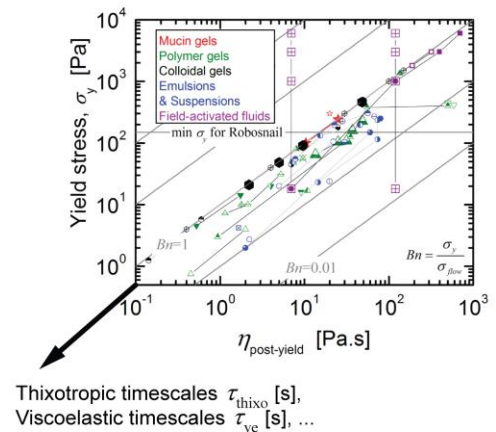Figure 2: Rheological property maps for viscoelastic, plastic, and thixotropic effects. (A) Cross-property plot of linear viscoelastic features including "springiness"; from (Davis 1937) (reused with permission from Cambridge University Press). (B) Cross-property plot of dynamic yield stress and post-yield viscosity at 10 s^{-1} for a wide survey of yield stress fluids (measured in steady shear flow, colors indicate different material classes, symbols differentiate each material). Additional axes can be included with a vision to add important timescales, both viscoelastic and thixotropic. Adapted from (Ewoldt et al. 2007; Ewoldt 2014) which describe materials in more detail.

Rheological property maps

As a first example of a rheological state map that sought to categorize and rank the response of a family of elastoviscoplastic materials, we show in Figure 2(A) a plot from (Davis 1937) during his studies of the viscoelasticity and springiness of cheese products. The abscissa

10

represents values of the shear viscosity η, logarithmically spaced as we do today, but displayed as values of pV $= \log_{10}(\eta)$, by analogy with the logarithmic spacing of pH (an interesting evolutionary rheological dead-end). The ordinate shows logarithmically spaced values of elasticity (or modulus, pM $= \log_{10}(G)$). Davis considered the linear and nonlinear creep response of cheese within the framework of a Maxwell model and correlated the viscoelastic relaxation time with the *technological property* (Reiner 1971) of 'springiness'. In the space of this material property map lines of constant viscoelastic relaxation time $t_{ve} = \eta/G$ thus correspond to 45˚ lines with equation $pS \equiv \log_{10}(\tau_{ve}) = pV - pM$. As Davis notes, *"this diagram epitomizes the plastic and elastic properties not only of cheese and butter but all similar materials."* Reiner & Scott Blair provide an extensive lexicon of descriptive terms such as 'springiness' and 'rubberiness' which they define to be *assessable* but not *measurable* (Reiner and Scott Blair 1967) as the flow conditions and kinematic history are not simple to define or control. Interestingly the language of fractional calculus appears to provide a way forward in quantifying such properties in the future (Faber et al. 2017).

Bingham would note that the plot in Figure 2(A) in fact conflates concepts of plastic flow (above a critical forcing amplitude) with creep (below a critical amplitude), and again this suggests that we are, in reality, looking at a projection of a three-dimensional representation as sketched generically in Figure 1(B). An alternate and more modern 2D projection of this design space that still captures many of the same spirits and features is shown in Figure 2(B), adapted from (Ewoldt 2014).

Figure 2(B) covers a wide survey of yield stress fluids, motivated by using these materials to achieve novel functionality in engineered systems. Specifically in (Ewoldt et al. 2007), the motivation was a wall-climbing robot, "Robosnail", inspired by the adhesive locomotion of

gastropods (snails and slugs). The map of Figure 2(B) is of course more generally useful for other scenarios in which yield stress fluids flow, such as particle stabilization, paint spray and impact, and additive manufacturing with direct ink writing processes. Logarithmically spaced values of the yield stress or critical stress S_y for onset of flow (or in the spirit of Davis, perhaps $pY = \log_{10}(\sigma_y)$) are shown against values of the post yield viscosity $\eta_{post-yield}$ (at a characteristic shear rate of 10 s^{-1}). A given application can select the best material from this cross-property plot, similar to Ashby's famous cross-property plots for material selection in design (Ashby 1999). For Robosnail, the ideal material would have a high yield stress but a low post-yield viscosity, i.e. the upper left portion of Figure 2(B). (We note that the data here are for dynamic yield stress during flow, rather than the static yield stress required to initiate flow, which is arguably equally relevant but not as generally available for the materials surveyed in Figure 2(B)). A high yield stress allows the robot to stick to walls, carry its own weight, and still push itself upward. A low post-yield viscosity helps the moving portions slide easily along the surface. The 45° lines in this design space are lines of constant *Bingham number* $Bn = \sigma_y / \eta_{post-yield} \dot{\gamma}_c$ (Bird et al. 1983). It can be seen that for most materials considered, the dynamic yield stress and the viscosity increase concomitantly, guiding design limitations for robot size and locomotion speed (for example, heavier wall-crawling robots will require larger yield stresses to resist gravity, but as a result will have to locomote over a more viscous liquid film, post yield). One might circumvent this trade-off by considering the *static* yield stress rather than the dynamic yield stress, although thixotropic timescales are a major concern for recovering a static yield stress. Another interesting mode for circumventing these limitations can be readily identified from this figure; switching the state of a field responsive material such as a magnetorheological or electrorheological fluid from field on (high yield stress) to field off (little or no yield stress)

can dramatically change the value of the Bingham number and the location within this design space.

The property map in Figure 2(B) is of course incomplete. These two descriptions of yield stress and post-yield viscosity do not describe the full complexity of the materials listed, e.g. one may be interested in elastic modulus before yield, or the yield strain, or, importantly to the robotic locomotion, the thixotropic restructuring timescale(s) of the material. The open literature has not yet organized rheological data as a collection of property maps. One challenge will be to use low-dimensional descriptions that are still adequate for complex, function-valued material properties. However complex the fluid, measurement of quantitative values of the relevant material properties are needed for construction of Pipkin maps which have dimensionless axes. Yet, Pipkin maps need not be dimensionless; in fact, keeping dimensional axes allows for mapping flow conditions in a given process of interest *independent* of the specific material to be used.
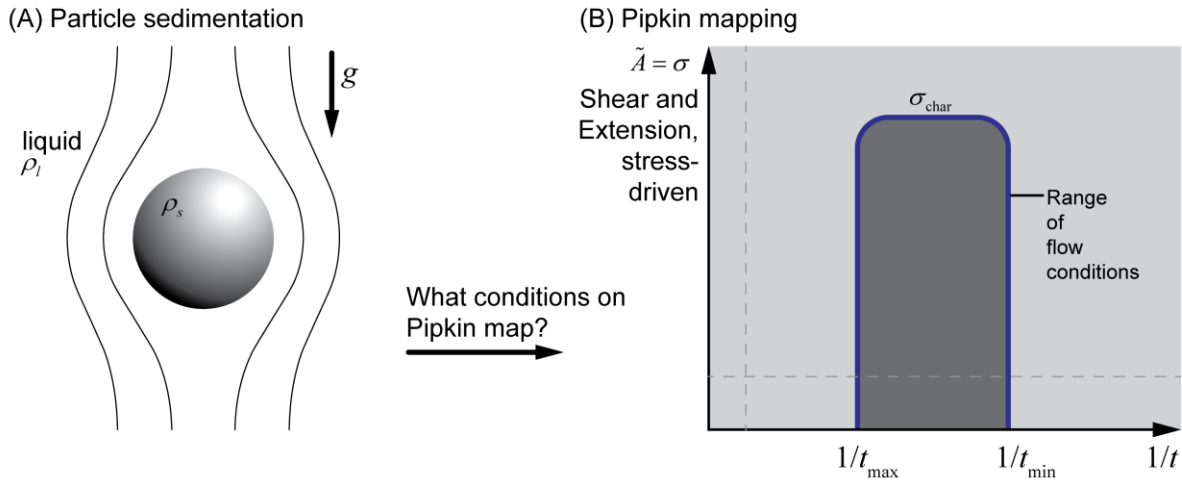
(A) Particle sedimentation

(B) Pipkin mapping

Figure 3. Flow conditions (A) can be mapped to a Pipkin space (B) and compared with limits of steady and linear regimes (dashed lines in (B)). Axes that are dimensional (rather than dimensionless), and careful choice of the amplitude for the vertical axis may help map flow conditions independent of the material involved. Here, for a sphere of radius R sedimenting due to gravity, the characteristic stress $\sigma_{char} \approx (\rho_s - \rho_l) g R$ is independent of the complex rheology of the surrounding liquid. The transient timescale t relates to the time for a sphere to move one particle diameter. Rheological characterization should use conditions relevant to such in-use conditions, e.g. stress-controlled nonlinear transient testing in both shear and extension; the steady flow regime may not even be relevant.

Flow conditions mapped to Pipkin space

Pipkin spaces with *dimensional* axes can be useful for helping to understand specific flow processes. That is, what transient timescales and deformation amplitudes are relevant in the flow of interest, be it pipe flow, swallowing, or a sedimenting sphere? To what extent can these flow conditions be identified independent of the material being processed?

Consider the flow conditions near a sedimenting sphere, as sketched in Figure 3. Mapping the flow conditions (amplitudes and transient timescales) to a Pipkin map will guide appropriate rheological characterization, and guide the appropriate conditions for calibrating (and selecting) constitutive models, a non-trivial task (Fraggedakis et al. 2016a; Fraggedakis et al. 2016b).

What amplitude should be chosen to represent the flow conditions: strain, strain-rate, or stress? We are often tempted to identify strain-rates that define the process. Here, *stress* is the natural choice, because it is independent of the liquid rheology. The state of stress is set by the

14

density mismatch of the sphere and the liquid, $\sigma_{char} \sim \dfrac{\Delta\rho g \forall}{Area} \sim \Delta\rho g R$, where $\forall$ is the volume

and R is the radius of the sedimenting sphere. This provides a characteristic measure of the largest stresses to be expected in the vicinity of the sphere (be it in a Newtonian fluid, or a complex TEVP material, whatever the value of yield stress). Fluid far from the sphere experiences stresses near zero, thus the range of applicable stress is shown schematically in Figure 3.

What transient timescale to use? This will depend on the rheological details of the fluid to be considered. One might however choose a characteristic transient timescale $t_c \sim R/U_{ss}$ characterized by the time for a sphere to travel one diameter at steady state. For fast flow, this may be 10 diameters per second (or higher). For slower sedimentation, it may travel only a fraction of a diameter per second. This general range, covering several orders of magnitude, is indicated schematically shown in Figure 3.

Having these expectations for the dynamic conditions in the flow near the sedimenting sphere, one can now choose the most relevant rheometric tests to probe the material rheology that are involved at these *timescales* and *stress* amplitudes. A reasonable choice may be step changes in shear stress (creep compliance and recovery) at different values of stress amplitude, or large amplitude oscillatory shear, which has been shown useful for model selection and calibration (Fraggedakis et al. 2016a; Fraggedakis et al. 2016b). Or, one may choose less-standard rheometric scheduling to mimic the process, e.g. ramping the imposed stress up and down over different timescales (Weber et al. 2012; Poumaere et al. 2014). Clearly, rheometric test conditions should match the expected flow conditions to be most informative. Using a similar dimensional Pipkin map, the rheological tests can also be mapped to ensure that they

15

cover the relevant flow kinematics (shear versus extension) and appropriate amplitudes and transient timescales.
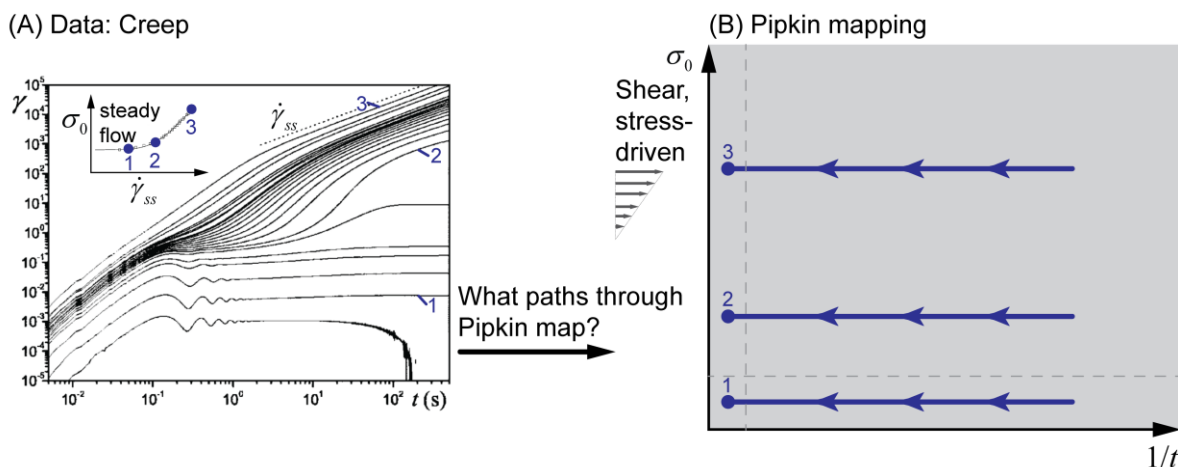

Figure 4. Rheometric conditions can be mapped to a Pipkin space. The type of deformation (e.g. shear or extension) and the controlled amplitude must be specified. (A) Experimental data from nonlinear creep compliance (step shear stress) of a thixotropic yield stress fluid (Bentonite suspension, adapted from (Coussot et al. 2006), their Figs. 1b, 8, Reprinted with permission. Copyright 2006, The Society of Rheology). (B) The rheometric test conditions define paths through the Pipkin map. Three examples are shown. Note that steady state conditions only describe the farthest left coast of the map, indicated with filled circles in both (A) and (B).

Rheometric test conditions mapped to Pipkin space

Any rheological characterization is a path through the Pipkin space. Typical rheological characterization specifies the kinematics of the flow field (e.g. simple shear, or uniaxial extension) and then controls an amplitude A (strain, strain-rate, or stress) as a function of time. The different choices of amplitude, and especially flow field, may require multiple Pipkin maps, composing something of a *Pipkin Atlas*.

Figure 4 shows one page of such an atlas for stress-controlled conditions in simple shear flow. Figure 4(A) shows the common visualization of the material response for a series of creep compliance (step stress) tests (adapted with permission from (Coussot et al. 2006)). Figure 4(B)

16

represents each of these tests as a path through a Pipkin space. The mapping helps emphasize the relevant limits for both linear viscoelasticity and the approach to steady flow. For example, when reading a paper wherein a single creep compliance curve is shown, the astute reader might picture in their mind the full Pipkin map to give perspective to the vast range of behavior possible that may not be captured by a single curve. Moreover, the Pipkin map re-emphasizes the locus of steady flow states which are confined to the left coast of the map. The approach to steady flow conditions may be quite complex; in this example shown in Figure 4(A) creep ringing (oscillatory response in the material strain) is observed at short times, followed by delayed yielding at long times.

We also suggest that Pipkin's framework be extended beyond just shear flow; extension and shear flow would then have different maps (akin to *two* amplitude axes, one for shear, one for extension). We know that behavior can be qualitatively different in shear compared to extension (e.g. for polymeric liquids shear-*thinning* versus extensional-*thickening* at large amplitudes of deformation). There is growing evidence of elastoviscoplastic yield stress fluids demonstrating rate-thinning in shear flows, but extensional-thickening responses in shear-free flows (Nelson 2015), yet the simplest models (e.g. the tensorial Bingham elasto-plastic model), as well as other test materials (e.g. Carbopol), show qualitatively similar behavior in both shear and extension,. For given flow conditions and materials of interest, these distinctions should be probed, not assumed, e.g. by considering both the "extensional amplitude" axis and "shear amplitude" axis of the Pipkin map. Of course near the lower corners of the plot, corresponding to Newtonian and linear viscoelastic materials, such kinematic distinctions between shear and extension are unnecessary (a proper tensorial constitutive treatment provides the interchangeability), but for nonlinear responses, both shear and extension may be quite distinct, and the material properties

17

may need to be determined as functions of both the second and third invariants of the rate of deformation tensor (Bird et al. 1987).
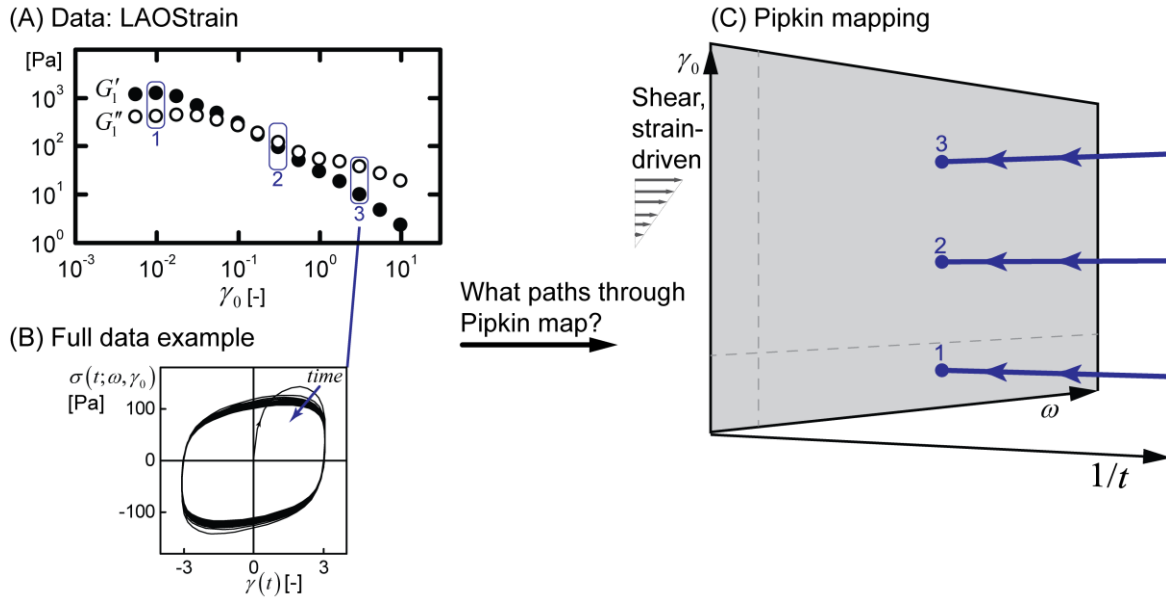

Figure 5. Large-amplitude oscillatory shear (LAOS) characterization data requires a 3-D Pipkin map using two transient time axes: frequency ω and transient time t. (A,B) Data from a thixotropic drilling mud (frequency $\omega = 15$ rad/s from (Ewoldt et al. 2010), data from their Figs. 1, 14, 15a). (B) Detailed plot of stress hysteresis during cyclic testing (represented as a Lissajous-Bowditch curve). In oscillatory deformation, key signatures of TEVP are observed, including (i) transient peak stress response decaying in time towards a periodic attractor, and (ii) Lissajous-Bowditch curves with stored and dissipated energy which evolve over timescales different than the stress relaxation time. The limit cycle behavior (known as the "alternance state") is the region most commonly analyzed, for which a two-dimensional Pipkin space can be used, highlighted in gray and with blue circles in (C), corresponding to data in (A).

As shown in Figure 5 for LAOS, an additional time axis may also be needed to map flow conditions to a Pipkin diagram. A typical LAOS amplitude sweep data is shown in Figure 5(A), here for a thixo-elasto-visco-plastic drilling mud (data from (Ewoldt et al. 2010)). Underlying each data point in Fig. 5(A) is raw oscillatory data that may be evolving over a transient timescale t to eventually reach this limit cycle behavior (a.k.a. the "alternance state" (Giacomin et al. 2011)).

18

A two-dimensional map of frequency and amplitude is commonly used to describe LAOS test conditions, indicated by the gray panel in Figure 5(C). While frequency and amplitude define the imposed test conditions, and conveniently map to Deborah and Weissenberg numbers respectively, an additional transient time scale is also involved. This is the total time t since the beginning of the oscillation, and can be used to create the additional axis as shown schematically in Fig. 5(C).

The transient evolving material behavior in LAOS can also be important, and deserves an additional axis on the Pipkin map. For example, in materials with both viscoelasticity and thixotropy, the material response at each instant (and its decomposition into elastic and viscous contributions) evolve during this global transient timescale. The material may be said to be *mutating* in time, as first considered by (Mours and Winter 1994). Specialized signal processing tools (such as the Gabor transform and/or short time Fourier transform (STFT) commonly used in digital speech processing) will be required for systematically deconvoluting temporal and frequency information. The three-dimensional version of Pipkin's map again helps us consider how transients and amplitude may elicit rheological complexity.

Figure 6 clarifies that some rheological flow fields are more complex than constant stress or strain rate and thus follow winding paths across the Pipkin map. We illustrate this by considering capillary-breakup extensional rheometry (CaBER) (McKinley 2005; Galindo-Rosales et al. 2013). Capillary forces drive the flow in this test, with the capillary stress increasing in time as the filament thins. In materials with yield stresses it is common to observe pronounced cusp-like regions during capillary thinning experiments as the deformation localizes near the pinch point. Mapping the trajectory of this stress forcing onto the Pipkin space helps give context to this rheological test. If material timescales are known, the axes can be made dimensionless, showing

the evolving values of the dimensionless groups during the test. Here too, the map gives a sense of place and context differentiating this and other tests that probe nonlinear and transient properties.

From the sample mappings in Figures 3-6, we hope the reader can see how to map any rheometric test, including frequency sweeps at fixed amplitude, nonlinear stress relaxation (similar to creep trajectories in Figure 3 but with strain amplitude on the ordinate), or large-amplitude oscillatory extension (Zhou and Schroeder 2016). Successful computations of complex flow fields in elastoviscoplastic fluids (see for example the recent work of (Fraggedakis et al. 2016a; Fraggedakis et al. 2016b)) need to calibrate the values of model parameters in relevant regions of the Pipkin map, co-locating test conditions and model parameters to the kinematic conditions expected in the flow domain of interest. It is thus of use to try and unify these different pages of a Pipkin atlas into a single holistic representation, in the same way that a globe integrates cartographic information and reveals connections hitherto hidden.
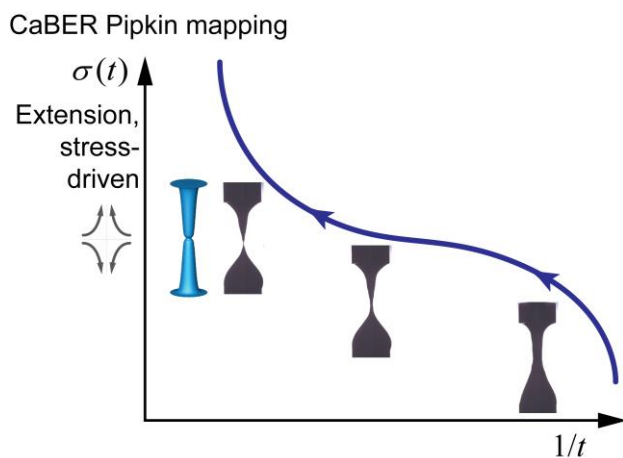

Figure 6. Non-constant amplitude trajectories through the Pipkin map occur for some rheological characterization flows. Here, Capillary-breakup extensional rheometry (CaBER) is a stress-driven flow due to capillary (surface tension) forces that increase in time. Inset images from TEVP material and model: Gray silhouette photos of oil-in-water emulsion with high volume fraction of internal phase (mayonnaise, previously unpublished experiments of Anna Park and Gareth H. McKinley); blue rendered image from simulation of a Soft Glassy Rheology (SGR) model of a "young" sample, adapted with permission from (Hoyle and Fielding 2015), their Fig.1, Copyrighted by the American Physical Society.

(A)

$Wi = \tau_{ve}\dot{\gamma}$

Thixoelastic Parameter

$$T_e = \frac{\tau_{ve}\dot{\gamma}}{\tau_{thixo}\dot{\gamma}} = \frac{\tau_{ve}}{\tau_{thixo}}$$

Elastoplastic Solid below yield

Elastoviscoplastic Fluid above yield

Bingham, HB

Thixoviscous Number

$\tau_{thixo}\dot{\gamma}$

Structural Parameter Models

Plastic Flow

$\tau_p\dot{\gamma}$ Thixoplastic number

(B)

$$\Sigma = \frac{\sigma}{\sigma_y}$$

Bingham, Herschel-Bulkley

Nonlinear elastoviscoplastic liquid above yield

Nonlinear elastoplastic solid below yield

Creep trajectories

Yield Surface

$\sigma_c\{\tau_e\omega, \tau_{thixo}\omega\}$

Linear viscoelastic solid

0

Deborah number $De = \tau_{ve}\omega$

Thixoviscous number

$$T_e = \frac{\tau_{ve}}{\tau_{thixo}}$$
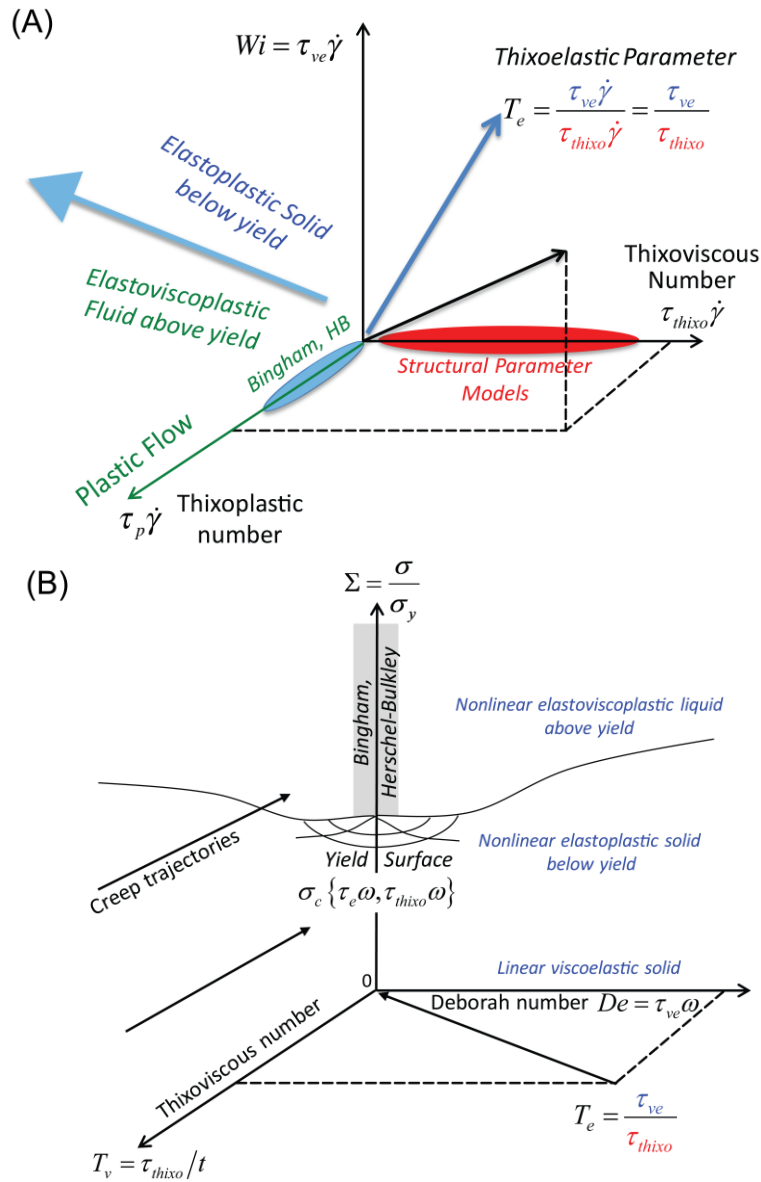
$T_v = \tau_{thixo}/t$

Figure 7. (A) TEVP materials represented in terms of three timescales. (B) A state space for TEVP Materials, created by extending Pipkin's map of nonlinear viscoelasticity to include thixotropic timescales; key features include a non-constant yield surface and rheometric flow trajectories with angle of approach toward the back corner determined by the ratio of viscoelastic to thixotropic timescales.

[Note to Press: please ensure these figures are typeset side by side across a full page (two columns width) in the final article proofs]

21

A Map for Thixo-Elasto-Visco-Plastic (TEVP) Materials & Models

Pipkin primarily used his map to organize the regions of applicability of predictive constitutive models. Nonlinear viscoelastic effects were considered, but *not* thixotropic timescales, nor explicit reference to plasticity. Based on the considerations we have discussed above, we use the Pipkin map as a foundation on which to construct a more general framework for comparing and ordering the response of Thixotropic Elasto-Visco-Plastic materials and the corresponding constitutive models.

One immediate issue that is faced as we seek to draw an appropriate map is the number of dimensions required to represent the most general response of a soft TEVP material; we can readily identify at least three different material time scales (associated with the response of the elastic, viscous and plastic material response) as well as the amplitude of the deformation (most typically the stress amplitude $S = S_0 / S_y$ where the yield stress scale S_y is a constant or reference value of the yield stress determined under a carefully specified shearing history or preparation protocol, e.g. the 'dynamic yield stress' of the material determined after a long period of steady shearing). We therefore require the ability to draw a four dimensional map! Rather than attempting to draw a Pipkin Hypercube (!) we thus consider here two different three-dimensional projections that we believe are useful. First in Figure 7(A), we sketch a three-dimensional parameter space for representing the three different time scales associated with a general thixotropic elastoviscoplastic (TEVP) material. In this space, clear distinctions are made between (i) the characteristic time scale on which the shear viscosity evolves (the thixotropic breakdown time scale, τ_{thixo} that typically appears in structural parameter models, such as those originating in the work of (Goodeve and Whitfield 1938; Moore 1959) and reviewed by (Mewis and Wagner 2009; Denn and Bonn 2011)), (ii) the viscoelastic time scale τ_{ve} on which elastic

stresses evolve, and which controls – for example – elastic recoil following the cessation of creep tests, and (iii) the time scale on which the yield stress is re-established following the cessation of flow, τ_p (often referred to as a thixotropic 'build up time' or 'restructuring time' or '*structuration time scale*'). The idealized inelastic models of Bingham and Herschel-Bulkley sit at the origin of this three-dimensional space in Figure 7(A). In his recent review, (Larson 2015) notes that "ideal thixotropic fluids" have instantaneous stress relaxation and no elastic recoil; they thus correspond to trajectories in the horizontal plane (with $De = 0$). Such materials may be difficult to realize in practice because the local interparticle attractive potentials that lead to flocculation and rigidity percolation will also give rise to viscoelastic responses at small strains (Jamali et al., 2017); however it is an important limit to study conceptually. We can define a "thixoviscous number" (i.e. the dimensionless measure of the relative importance of thixotropy at a given shear rate) as $T_v = \tau_{thixo}\dot{\gamma}$, and this dimensionless product is commonly encountered in purely thixoviscous "structural parameter models" (as discussed by (Larson 2015)). In these models the state of the material microstructure is projected down to a single scalar parameter (commonly denoted λ) which evolves with the material's deformation history. A large number of empirical structural parameter models exist and they commonly propose a simple direct relationship between the evolution of the yield stress $\mathcal{S}_y(\lambda(t))$, and the viscosity $\eta(\lambda(t))$. They thus correspond to prescribed trajectories through this plane. Many variants of this relationship have been proposed and discussed by Thompson and de Sousa Mendez; for reviews of these models see (de Souza Mendes and Thompson 2012; de Souza Mendes and Thompson 2013).

The relative ratio of any pair of the time scales shown in Figure 7(A) provides the slopes of material trajectories through this three-dimensional TEVP space as the imposed shear rate on the material is increased; for example, the ratio of the Deborah Number to the Thixoviscous number

results in a 'thixoviscoelastic parameter' $T_e = \tau_{ve}/\tau_{thixo}$ which is independent of the flow strength and is an intrinsic property of a thixotropic viscoelastic material. This has been considered by (Blackwell and Ewoldt 2014) in studies of LAOS flow of a viscoelastic, thixotropic yield stress model. Classical linear and nonlinear viscoelastic models are clustered along the ordinate (vertical) axis where $T_e \to \infty$. However, recently (Renardy 2010) and (Maki and Renardy 2010) have also considered nonlinear viscoelastic constitutive models which have two distinct stress relaxation processes and thus effectively two viscoelastic time scales. By allowing these time scales to be very widely separated they show that they can emulate the time-dependent yield-like response of soft solids (see (Renardy and Renardy 2016) for a recent overview). Larson (Larson 2015) has also considered this same limit for the Rolie-Poly model of polymer reptation, and carefully distinguishes between true thixotropy, which only affects the viscosity (and maybe the modulus) and viscoelasticity which results in long-time evolution of the viscoelastic stresses.

An interesting exercise is to attempt to specify the loci of different materials in this three dimensional TEVP space. For many materials (such as Carbopols and other swollen microgels) the thixotropic time scale is much larger than the viscoelastic one, i.e. $\tau_{thixo} \gg \tau_{ve}$ or $T_e \ll 1$; however, for certain Carbopol grades and special preparation histories (Dinkgreve et al. 2016) it is possible to prepare more ideal elastoplastic materials (corresponding to the left hand plane) which have no measurable thixotropy (at least on timescales accessible to current experimental methods). The limit of a purely inelastic thixoviscous material response (with $De \to 0$) is difficult to achieve; however perhaps the best examples of such materials are the high ionic strength flocculated waste slurries and 'cementitious' pastes that are encountered in nuclear waste handling streams (see for example, (Tracey et al. 1996; Chung et al. 2013)).

For more complex materials such as many consumer products, attractive gels, and complex fluids such as waxy crude oils, all three time scales may be important and typically $\tau_{thixo} \gg \tau_p > \tau_{ve}$ so that there is an initial viscoelastic response followed by the development of a yield stress and, ultimately, a long term evolution or 'rheological aging' in the properties of the system. In such systems a clear specification of the entire sample history is essential to ensure that the material response is independent of its preparation or its loading history (see (Fielding et al. 2000) for a clear discussion of such 'waiting time' effects). Many liquid-dispensed foods (e.g. squeezable mayonnaise or ketchup) on the other hand are designed to ensure that $t_p \ll t_{ve} \ll t_{thixo}$, so that a yield stress develops almost immediately after dispensing (and shearing), followed by viscoelastic stress relaxation on intermediate timescales, and possibly thixoviscous restructuring events under steady shearing; similar behavior can also be observed in biological gels (such as gastropod mucus, mucin gels). Designing robust test protocols to capture this rapid recovery in the material yield stress following cessation of shearing is an active area of current research, e.g. by using high frequency LAOS tests to access short timescale information based on predictions for the unique signatures of thixotropy (Blackwell and Ewoldt 2014).

Because very few studies to date have attempted to quantify all three of these time scales associated with recovery of the material yield stress (t_p), the fluid viscoelasticity (t_{ve}) and the time scale for thixotropic breakdown (τ_{thixo}), an alternate three-dimensional projection of this TEVP material space can be drawn to enable us to quantify the amplitude of the forcing experienced by the fluid. Because the elastic modulus, viscosity, and yield stress of the fluid are often all represented as functions of the structural parameter and its dependence on the shear protocol history $\lambda(t, \dot{\gamma}_0)$, a convenient approach is to conflate the plastic and thixotropic axes,

and replace the third axis with a dimensionless stress amplitude, $S_0 = S_0/S_y$, as shown schematically in Figure 7(B). We finally arrive at a generalization of Pipkin's original drawing suitable for capturing the TEVP response of soft solid materials.

In this drawing, viscoelasticity is parameterized by the Deborah number $De = \tau_{ve}\omega$ (or $De = \tau_{ve}/t$ for a more general time-dependent deformation) and thixotropic effects by the thixoviscous parameter $T_v = \tau_{thixo}/t$. The classical inelastic and non-thixotropic yield stress models proposed by Bingham and Herschel-Bulkley are then located along the ordinate axis for stresses $\Sigma \geq 1$. However, for general thixotropic soft solids, the critical stress above which the material yields and flows as a liquid is then represented by a (dimensionless) yield surface $\Sigma(\tau_{ve}/t, \tau_{thixo}/t)$. This surface can perhaps be most readily mapped out using large amplitude oscillatory stress (LAOStress) measurements with a suitable range of different input frequencies, $\Sigma(\tau_{ve}\omega, \tau_{thixo}\omega)$. We have also indicated that in general this yield surface is not a flat plane. For example the creep compliance trajectories shown in Figure 4(A) indicate that at low stresses $(\Sigma < 1)$ the material creeps but remains unyielded, whereas for conditions close to the critical stress $(\Sigma \approx 1)$ a thixotropic yield stress material may undergo transition from unyielded to yielded as time progresses and deformation accumulates. For clarity we have represented these creep trajectories on the left hand face of this TEVP state space in Figure 7(B); however we note that for a given material (e.g. a specific grade of carbopol gel at a specified pH, or a specific concentration of colloidal clay) the thixoelastic parameter T_e (i.e. the ratio of the elastic and thixotropic time scales) for the material is constant and so trajectories in fact evolve along specific vertical planes in this parameter space with azimuthal angle set by $T_e = \tau_{ve}/\tau_{thixo}$. So-

called "ideal yield stress materials" which exhibit no thixotropy (e.g. certain grades of carbopol gel) correspond to the rear plane of this space (with $T_v = 0$).

Constitutive Models for Elastoviscoplastic Materials

One area of intense recent interest is the development of appropriate rheologically-invariant constitutive models that can describe the range of material responses that are observed in different thixotropic elastoviscoplastic (TEVP) materials. Such models need to describe the different trajectories through the extended Pipkin space we have discussed above in terms of a set of coupled evolution equations for the internal microstructure of the material and the resulting macroscopic stress field. The material constants or functions that enter these models can be determined by carefully specifying the specific trajectories to be studied (e.g. creep tests at constant stress, or steady shear flow sweeps over a range of imposed shear rates), this is the domain of *rheometry*. Having fully determined these constants and functions, the aim of *non-Newtonian fluid dynamics* is to predict the response of such materials in more complex flow fields; for example the mixed shearing/extensional flow past a sphere (cf. Fig 3) or the start up of steady Poiseuille flow in a long pipe filled with a thixotropic yield stress material (such as a drilling mud or a waxy crude oil). It is not the goal of this perspective article to provide a detailed review of these developments; de Souza Mendes & Thompson provide a comprehensive overview of the state of the field for thixotropic inelastic fluids (corresponding to $T_e \rightarrow 0$) (de Souza Mendes and Thompson 2012), and Saramito (2009) has developed a general elastoviscoplastic formulation that unites the Bingham/Herschel-Bulkley (viscoplastic) and Oldroyd (quasi-linear viscoelastic) formulations in the absence of thixotropy (corresponding to $T_e^{-1} \rightarrow 0$). Elsewhere in this Special Issue the articles by Mitsoulis and Tsamopoulos (2017) and

27

by Saramito and Wachs (2017) discuss recent progress in using such models for numerically simulating complex flows of yield stress fluids.

To contrast and complement those other works, here we highlight one broad class of nonlinear elastoviscoplastic constitutive models that can capture, at least qualitatively, both thixotropy and elastoviscoplasticity (and therefore span the range of thixoviscoelastic parameters $0 \leq T_e \leq \infty$, covering the full range of the expanded Pipkin map in Fig. 7). This *Isotropic Kinematic Hardening* (or IKH) model framework has been introduced and discussed elsewhere (Dimitriou et al. 2013; Dimitriou and McKinley 2014). From an etymological viewpoint the name of this framework captures two key ideas; that both the central point (or locus) and the extent of the yield surface (for example represented in the form of Mohr's circle of principal stresses) will evolve with the material deformation history (*kinematic hardening)* and with the material's age (i.e. thixotropy or *isotropic hardening*). Here we briefly review the basic structure of the governing constitutive equations.

In the simplest form of the IKH model, the total stress in the material is represented in terms of an elastic, or viscoelastic, contribution to the deformation and a nonlinear plastic contribution that combine additively so that the total strain is $\gamma = \gamma_{ve} + \gamma_p$ and the stress in each mechanical element is the same, $\sigma = \sigma_{ve} = \sigma_p$. Below the yield stress the viscoelastic solid response of the material can be represented by *any* suitably frame-invariant constitutive expression of Maxwell/Kelvin-Voigt form inter-relating σ_{ve} and γ_{ve}. The state of the microstructure in the material is captured by a scalar parameter $\lambda(\dot{\gamma}(t'))$ and a tensorial quantity that is termed the *back stress* which also evolves with the time-varying deformation history experienced by the material. Physically, this tensor attempts to capture the evolution and anisotropic distribution of the defects (and resulting state of stress) that develop within the soft solid as it deforms. This

28

internal state of stress is generically represented in terms of a frame-invariant strain-like tensor $\mathbf{A}$ and a back-stress modulus C so that the back stress is $\sigma_{back} = C\mathbf{A}$. In a simple one-dimensional shearing flow, the 'flow rule' governing the macroscopic evolution of the plastic strain rate and the shear stress in the system is then given by

$$\dot{\gamma}_p = \left|\dot{\gamma}_p\right| \mathbf{e}_p \tag{1}$$

$$\left|\dot{\gamma}_p\right| = \left(\frac{\left|\sigma - \sigma_{back}\right| - \sigma_y}{\mu_p}\right)^{1/m} \qquad \text{if } \left|\sigma - \sigma_{back}\right| \geq \sigma_y \tag{2}$$

where $(\sigma - \sigma_{back})$ is the effective stress driving the evolution of the irreversible plastic strain in the material and $\mathbf{e}_p = (\sigma - \sigma_{back})/\left|\sigma - \sigma_{back}\right|$ sets the *directionality* of the effective stress in the material (tracking this directionality can be critically important in time-reversing flows such as LAOS). In equation (2), σ_{back} sets the dynamic yield stress of the material (after extended periods of steady shearing), σ_y is an *additional* contribution to the static yield stress of the material (which is expected to be a function of the internal microstructure, λ), μ_p is a (generalized) plastic viscosity with units of $[Pa.s^m]$ (equivalent to the consistency K in the Herschel-Bulkley model) and $0 < m \leq 1$ sets the nonlinearity of the macroscopic flow rule. The evolution of the back stress $\sigma_{back} = C\mathbf{A}$ is then connected to the evolution of the microstructure in the material through evolution equations of the form:

$$\dot{A} = \dot{\gamma}_p - \left(\left|A\right|q\right)^v sign(A)\left|\dot{\gamma}_p\right| \tag{3}$$

$$\dot{\lambda} = \frac{1}{\tau_p}(1 - \lambda) - \beta_y \lambda \left|\dot{\gamma}_p\right| \tag{4}$$

where the overdot indicates a time derivative. In these equations q, v, β_y, μ_p and k are constitutive model parameters (see Dimitriou and McKinley (2014) for details of how they can be determined from start-up of steady shear flow and/or LAOS deformations). The static

contribution to the yield stress is related to the degree of microstructure remaining in the material at any time t through a function of the form $\sigma_y = f(\lambda)$. Often the simplest possible linear relationship $\sigma_y = k\lambda$ is sufficient to capture, at least qualitatively, the effects of thixotropy and internal restructuring on changes in the magnitude of the yield stress. However, more general nonlinear forms can also be considered, and the evolution equation for the microstructural variable λ can also be connected to measures such as the fractal connectivity of the underlying microstructure (Mohraz and Solomon 2005; Geri et al. 2017).

The key feature to recognize in these evolution equations (3) and (4) for the defects and overall level of microstructure, respectively, is the dynamical balance between the first (creation) and second (nonlinear destruction) terms on the right hand side of each equation. In eq. (4) a fully structured material at equilibrium and under rest conditions corresponds to $\lambda = 1$ whilst prolonged shearing leads to thixotropy and a progressive loss of microstructure. Nondimensionalization of the equation using τ_{thixo} as the characteristic time scale immediately leads to a thixoviscous number $T_v = \tau_{thixo} |\dot{\gamma}_p|$. Alternatively if the equations are non-dimensionalized with the viscoelastic time scale (appearing in the separate constitutive equation for σ_{ve}) then the thixoviscoelastic ratio of time scales $T_e = \tau_{ve}/\tau_{thixo}$ immediately appears. In the IKH formulation the evolution of the back stress or defect strain (equation (3)) is not characterized by a separate, additional time scale but is associated purely with the kinematics of the external rate of shearing (i.e. with time scale $\sim \dot{\gamma}^{-1}$).

Full frame-invariant three-dimensional generalizations of these expressions are given in the supporting information of Dimitriou et al. (2014). The tensorial quantity A can be related to an elastic free energy function (see (Dimitriou et al. 2013) Appendix B, and (Ames et al. 2009) for

additional details) and therefore more complex relationships than a direct linear relationship between the components of the back stress tensor and *A* can easily be developed; such functional forms have not yet been explored in detail but may be very important for capturing nonlinear elastic effects during rapid transient flows such as LAOS or shear start up flows (see the work by (Dinkgreve et al. 2017) elsewhere in this special issue for examples of the latter test protocol).

The coupled equations (1) – (4) (combined with an appropriate constitutive expression for the viscoelastic stress σ_{ve}) can capture many of the key Thixo-Elasto-Visco-Plastic features we have described in this perspective article. In particular, the steady state flow curve becomes non-monotonic with different values of the static and dynamic yield stress, start up of steady shear produces large stress overshoots, and LAOS deformations result in non-elliptical Lissajous-Bowditch curves as well as stress overshoot and a slow (multicycle) thixotropic decay towards the final 'alternance state' as can be observed in Figure 5B (see (Dimitriou and McKinley 2014) for details).

If $k = \beta_y = 0$, then there is no isotropic hardening or restructuring of the material and the magnitude of the yield stress does not evolve with time; however the locus of the center of the yield stress surface can still evolve with the kinematical flow history and this is now captured by the evolution in the internal 'back stress' S_{back} in the material. If $\nu = 1$ then the resulting *Kinematic Hardening* (*KH*) equations can be solved analytically (see (Dimitriou et al. 2013)) and at steady state ($\dot{A} \to 0$) the material response predicted by eqs. (1) – (3) becomes identical to the Herschel-Bulkley model with a critical stress (or dynamic yield stress) $\sigma_c = C/q$. Careful experimental measurements of the local fluidization in simple yield stress materials also reveal this approach towards a limiting Herschel-Bulkley rheological response at long times, and the

index *m* can be related to the ratio of non-trivial fluidization exponents determined in constant shear rate and constant stress protocols ((Divoux et al. 2011)).

In controlled stress deformations, however, the KH model also captures transient viscoelastoplastic features such as the one we have sketched generically in Figure 4(B). Specifically, for imposed stresses $\sigma_0 > \sigma_c$, the material flows like a viscous liquid at steady state; however for smaller stresses   the material creeps or plastically flows with an apparent viscosity $\eta^+ = \sigma_0 / \frac{d\gamma_p}{dt}$ that diverges as a power law in time (Dimitriou et al. 2013) because the instantaneous rate of shearing slowly approaches zero. (Parenthetically we note that a more natural variable (also discussed by Bingham in his original paper a century ago) to plot on the ordinate would be the *apparent fluidity* $\phi^+ = \frac{1}{\sigma_0} \frac{d\gamma_p}{dt}$, which approaches zero in the limit of long times and small stresses). In Figure 8 we show the resulting form of the flow curves (projected onto a two dimensional plane) as we pick progressively longer values of the elapsed time, as well as corresponding experimental observations by (Møller et al. 2009) for an ideal elastoplastic grade of carbopol that doesn't exhibit thixotropic effects.

It becomes clear that the sharp demarcation of viscous flow from plastic flow, originally sought by Bingham one hundred years ago, is in fact somewhat ephemeral, and a function of not only the stress imposed but also the total time elapsed in the experiment.
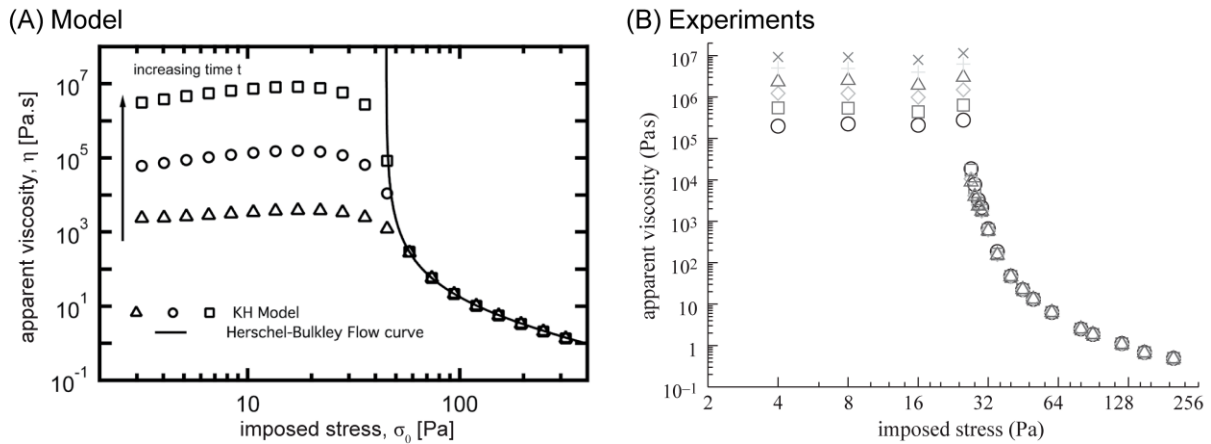
Figure 8. Evolution of the apparent viscosity $\eta^+ = \sigma_0/\dot{\gamma}(t)$ for (A) the kinematic hardening model with a critical yield stress of $\sigma_c = C/q = 45\,\text{Pa}$. Above the critical stress, the apparent viscosity is independent of the elapsed time, and the kinematic hardening model reduces to the Herschel-Bulkley flow curve. However, at lower stresses, the viscosity diverges in time. (B) The corresponding experimental measurements as observed in a Carbopol gel showing a 'simple yield stress' (i.e. non-thixotropic) response, adapted from (Møller et al. 2009).
[Note to Press: please ensure these figures remain side by side across a full page (two columns width)]

Conclusions

In this work we have attempted to show how the concepts of plasticity and thixotropy can be incorporated with viscoelasticity and described using higher dimensional Pipkin maps. Moreover, this augmented thixo-elasto-visco-plastic Pipkin space allows for mapping flow conditions to rheological test conditions, and this can help isolate different transient behaviors in the flow and in the material. We have therefore seen how such Pipkin maps help to organize (i) flow/in-use conditions, (ii) rheometric protocols, and (iii) predictive constitutive models. We note that a *dimensional* Pipkin map can be enough, especially for the first two uses enumerated above; however a truly dimensionless TEVP Pipkin map requires determination of viscoelastic

33

and thixotropic time scales using appropriate rheological test histories, as discussed by (Mewis and Wagner 2009) and (Larson 2015).

We hope these expanded views of Pipkin's original map will help researchers identify new ways to organize and describe the rheological complexity of thixotropic elastoviscoplastic materials. For example, developing projections such as those sketched in Figure 7 for different classes of soft solids may help provide reminders of model limitations and regions of applicability, identify different limiting regimes of material behavior, and the range of conditions that can be explored with a given rheological characterization protocol. Pipkin's original paradigm of ordering and distinguishing between different transient and nonlinear conditions gives us a foundation to build upon as we begin to explore and organize the world of rheological complexity in soft solids such as colloidal gels and clay dispersions which not only exhibit nonlinear viscoelasticity and thixotropy, but also the pronounced plastic response that inspired Bingham's original work one hundred years ago.

Acknowledgements

References

Ames NM, Srivastava V, Chester SA, Anand L (2009) A thermo-mechanically coupled theory for large deformations of amorphous polymers. Part II: Applications. Int J Plast 25:1495–1539. doi: 10.1016/j.ijplas.2008.11.005

Ashby MF (1999) Materials selection in mechanical design. Butterworth-Heinemann, Boston, MA

Astarita G, Jongschaap RJJ (1978) The maximum amplitude of strain for the validity of linear viscoelasticity. J Nonnewton Fluid Mech 3:281–287. doi: 10.1016/0377-0257(78)87005-0

Balmforth NJ, Frigaard IA, Ovarlez G (2013) Yielding to Stress: Recent Developments in Viscoplastic Fluid Mechanics. Annu Rev Fluid Mech 46:130819114955006. doi: 10.1146/annurev-fluid-010313-141424

Barnes HA (1997) Thixotropy - A review. J Nonnewton Fluid Mech 70:1–33.

Bharadwaj NA, Ewoldt RH (2014) The general low-frequency prediction for asymptotically-nonlinear material functions in oscillatory shear. J Rheol (N Y N Y) 58:891–910.

Bharadwaj NA, Ewoldt RH (2015) Constitutive model fingerprints in medium-amplitude oscillatory shear. J Rheol (N Y N Y) 59:557–592. doi: 10.1122/1.4903346

Bingham EC (1916) An Investigation of the Laws of Plastic Flow. In: Bulletin of the Bureau of Standards, Vol. 13, No. 2. Govt. Print. Off.., Washington, pp 309–353

Bird RB, Armstrong RC, Hassager O (1987) Dynamics of Polymeric Liquids: Volume 1 Fluid Mechanics, 2nd Ed. John Wiley and Sons, Inc, New York

Bird RB, Dai G, Yarusoo BJ (1983) The rheology and flow of viscoplastic materials. Rev Chem Eng 1:1–70. doi: 10.1515/revce-1983-0102

Blackwell BC, Ewoldt RH (2014) A simple thixotropic-viscoelastic constitutive model produces unique signatures in large-amplitude oscillatory shear (LAOS). J Nonnewton Fluid Mech 208:27–41. doi: 10.1016/j.jnnfm.2014.03.006

Bonn D, Paredes J, Denn MM, et al (2015) Yield Stress Materials in Soft Condensed Matter. arXiv:1502.05281.

Boromand A, Jamali S, Maia M (2017) Structural fingerprints of yielding mechanisms in attractive colloidal gels. Soft Matter 13:458–473. doi: 10.1039/c6sm00750c

Carter KA, Girkin JM, Fielding SM (2016) Shear banding in large amplitude oscillatory shear (LAOStrain and LAOStress) of polymers and wormlike micelles. J Rheol (N Y N Y) 60:883–904. doi: 10.1122/1.4960512

Chung C, Chun J, Um W, et al (2013) Setting and stiffening of cementitious components in Cast Stone waste form for disposal of secondary wastes from the Hanford waste treatment and immobilization plant. Cem Concr Res 46:14–22. doi: 10.1016/j.cemconres.2013.01.003

Coussot P, Tabuteau H, Chateau X, et al (2006) Aging and solid or liquid behavior in pastes. J Rheol (N Y N Y) 50:975. doi: 10.1122/1.2337259

Davis JG (1937) 162. The Rheology of Cheese, butter and Other Milk Products (The Measurement of "Body" and "Texture"). J Dairy Res 8:245–264. doi: 10.1017/S0022029900002090

Davis WM, Macosko CW (1978) Nonlinear Dynamic Mechanical Moduli for Polycarbonate and PMMA. J Rheol (N Y N Y) 22:53–71.

Dealy JM (2010) Weissenberg and Deborah Numbers - Their Definition and Use. Rheol Bull 79:14–18.

Dealy JM, Wissbrun KF (1990) Melt rheology and its role in plastics processing: theory and applications. Van Nostrand Reinhold, New York

de Souza Mendes PR, Thompson RL (2012) A critical overview of elasto-viscoplastic thixotropic modeling. J Nonnewton Fluid Mech 187–188:8–15. doi: 10.1016/j.jnnfm.2012.08.006

de Souza Mendes PR, Thompson RL (2013) A unified approach to model elasto-viscoplastic thixotropic yield-stress materials and apparent yield-stress fluids. Rheol Acta 52:673–694. doi: 10.1007/s00397-013-0699-1

Denn MM, Bonn D (2011) Issues in the flow of yield-stress liquids. Rheol Acta 50:307–315. doi: 10.1007/s00397-010-0504-3

Dimitriou CJ, Ewoldt RH, McKinley GH (2013) Describing and prescribing the constitutive response of yield stress fluids using large amplitude oscillatory stress (LAOStress). J Rheol (N Y N Y) 57:27–70. doi: 10.1122/1.3684751

Dimitriou CJ, McKinley GH (2014) A comprehensive constitutive law for waxy crude oil: a thixotropic yield stress fluid. Soft Matter 10:6619–44. doi: 10.1039/c4sm00578c

Dinkgreve M, Bonn D, Denn MM (2017) "Everything flows?" Elastic effects on start-up flows of yield stress fluid.

Dinkgreve M, Paredes J, Denn MM, Bonn D (2016) On different ways of measuring "the" yield stress. J Nonnewton Fluid Mech. doi: 10.1016/j.jnnfm.2016.11.001

Divoux T, Barentin C, Manneville S (2011) From stress-induced fluidization processes to Herschel-Bulkley behaviour in simple yield stress fluids. Soft Matter 7:8409–8418. doi: 10.1039/c1sm05607g

Ewoldt RH (2014) Extremely soft: design with rheologically complex fluids. Soft Robot 1:12–20. doi: 10.1089/soro.2013.1508

Ewoldt RH (2016) Predictions for the northern coast of the shear rheology map: XXLAOS. J Fluid Mech 798:1–4. doi: 10.1017/jfm.2016.265

Ewoldt RH, Bharadwaj NA (2013) Low-dimensional intrinsic material functions for nonlinear viscoelasticity. Rheol Acta 52:201–219. doi: 10.1007/s00397-013-0686-6

Ewoldt RH, Clasen C, Hosoi AE, McKinley GH (2007) Rheological fingerprinting of gastropod pedal mucus and synthetic complex fluids for biomimicking adhesive locomotion. Soft Matter 3:634–643. doi: 10.1039/b615546d

Ewoldt RH, Gurnon AK, López-Barrón C, et al (2012) LAOS Rheology Day, Friday the 13th, Colburn Laboratory, University of Delaware.

Ewoldt RH, Hosoi AE, McKinley GH (2008) New measures for characterizing nonlinear viscoelasticity in large amplitude oscillatory shear. J Rheol (N Y N Y) 52:1427–1458. doi: 10.1122/1.2970095

Ewoldt RH, Winter P, Maxey J, McKinley GH (2010) Large amplitude oscillatory shear of pseudoplastic and elastoviscoplastic materials. Rheol Acta 49:191–212.

Faber TJ, Jaishankar A, McKinley GH (2017) Describing the firmness, springiness and rubberiness of food gels using fractional calculus. Part I: Theoretical framework. Food Hydrocoll 62:311–324. doi: 10.1016/j.foodhyd.2016.05.041

Fielding SM, Sollich P, Cates ME (2000) Aging and rheology in soft materials. J Rheol (N Y N Y) 44:323–369.

Fraggedakis D, Dimakopoulos Y, Tsamopoulos J (2016a) Yielding the yield stress analysis: A thorough comparison of recently proposed elasto-visco-plastic (EVP) fluid models. J Nonnewton Fluid Mech 236:104–122. doi: 10.1016/j.jnnfm.2016.09.001

Fraggedakis D, Dimakopoulos Y, Tsamopoulos J (2016b) Yielding the yield-stress analysis: a study focused on the effects of elasticity on the settling yield-stress fluids. Soft Matter 12:5378–5401. doi: 10.1039/C6SM00480F

Galindo-Rosales FJ, Alves MA, Oliveira MSN (2013) Microdevices for extensional rheometry of low viscosity elastic liquids: A review. Microfluid Nanofluidics 14:1–19. doi: 10.1007/s10404-012-1028-1

Geri M, McKinley GH, Venkatesan R, Sambath K (2017) Thermo-Kinematic Memory and the Thixotropic Elasto-Visco-Plasticity of Waxy Crude Oils. J Rheol (N Y N Y) 61:in press.

Giacomin AJ, Bird RB, Johnson LM, Mix AW (2011) Large-amplitude oscillatory shear flow from the corotational Maxwell model. J Nonnewton Fluid Mech 166:1081–1099. doi: 10.1016/j.jnnfm.2011.04.002

Goodeve CF, Whitfield GW (1938) The measurement of thixotropy in absolute units. Trans Faraday Soc 34:511–520. doi: 10.1039/TF9383400511

Hoyle DM, Fielding SM (2015) Age-Dependent Modes of Extensional Necking Instability in Soft Glassy Materials. Phys Rev Lett 114:158301. doi: 10.1103/PhysRevLett.114.158301

Hyun K, Wilhelm M, Klein CO, et al (2011) A review of nonlinear oscillatory shear tests: Analysis and application of Large Amplitude Oscillatory Shear (LAOS). Prog Polym Sci 36:1697–1753. doi: 10.1016/j.progpolymsci.2011.02.002

Jamali S, McKinley GH, Armstrong RC (2017) Microstructural Rearrangements and their Rheological Implications in a Model Thixotropic Elastoviscoplastic Fluid. Phys Rev Lett 118:48003. doi: 10.1103/PhysRevLett.118.048003

Khair AS (2016a) On a suspension of nearly spherical colloidal particles under large-amplitude oscillatory shear flow. J Fluid Mech 791:R5. doi: 10.1017/jfm.2016.77

Khair AS (2016b) Large amplitude oscillatory shear of the Giesekus model. J Rheol (N Y N Y) 60:257–266. doi: 10.1122/1.4941423

Larson RG (2015) Constitutive equations for thixotropic fluids. J Rheol (N Y N Y) 59:595–611. doi: 10.1122/1.4913584

Macosko CW (1994) Rheology : principles, measurements, and applications. Wiley-VCH, New York

Maki KL, Renardy Y (2010) The dynamics of a simple model for a thixotropic yield stress fluid. J Nonnewton Fluid Mech 165:1373–1385. doi: 10.1016/j.jnnfm.2010.07.002

McKinley GH (2005) Visco-elasto-capillary thinning and break-up of complex fluids. In: Binding DM, Walters K (eds) Annual Rheology Reviews. British Society of Rheology, pp 1–48

Mewis J, Wagner NJ (2009) Thixotropy. Adv Colloid Interface Sci 147–148:214–27. doi: 10.1016/j.cis.2008.09.005

Mitsoulis E, Tsamopoulos JA (2017) Numerical Simulations of Complex Yield Stress Fluid Flow.

Mohraz A, Solomon MJ (2005) Orientation and rupture of fractal colloidal gels during start-up of steady shear flow. J Rheol (N Y N Y) 49:657–681. doi: 10.1122/1.1895799

Møller P, Fall A, Chikkadi V, et al (2009) An attempt to categorize yield stress fluid behaviour. Philos Trans A Math Phys Eng Sci 367:5139–55. doi: 10.1098/rsta.2009.0194

Moore F (1959) The rheology of ceramic slips and bodies. Trans Br Ceram Soc 58:470–494.

Mours M, Winter HH (1994) Time-resolved rheometry. Rheol Acta 33:385–397. doi: 10.1007/BF00366581

Nelson AZ (2015) Extending yield-stress fluid paradigms. University of Illinois at Urbana-Champaign

Osswald TA, Rudolph N (2015) Polymer Rheology : Fundamentals and Applications. Hanser Publications, Cincinnati

Papanastasiou TC (1987) Flows of materials with yield. J Rheol (N Y N Y) 31:385–404.

Pipkin AC (1972) Lectures on Viscoelasticity Theory. Springer, New York

Poumaere A, Moyers-gonzález M, Castelain C, Burghelea T (2014) Unsteady laminar flows of a Carbopol gel in the presence of wall slip. J Nonnewton Fluid Mech 205:28–40. doi: 10.1016/j.jnnfm.2014.01.003

Reimers MJ, Dealy JM (1996) Sliding plate rheometer studies of concentrated polystyrene solutions: Large amplitude oscillatory shear of a very high molecular weight polymer in diethyl phthalate. J Rheol (N Y N Y) 40:167–186.

Reimers MJ, Dealy JM (1998) Sliding plate rheometer studies of concentrated polystyrene solutions: Nonlinear viscoelasticity and wall slip of two high molecular weight polymers in tricresyl phosphate. J Rheol (N Y N Y) 42:527–548.

Reiner M (1971) Advanced rheology. H.K. Lewis, London

Reiner M, Scott Blair GW (1967) Rheology terminology. In: Fisiol FR (ed) Rheology Vol. 4. Academic Press, New York, pp 461–488

Renardy M (2010) The mathematics of myth : Yield stress behavior as a limit of non-monotone constitutive theories. J Nonnewton Fluid Mech 165:519–521. doi: 10.1016/j.jnnfm.2010.02.010

Renardy M, Renardy Y (2016) Thixotropy in yield stress fluids as a limit of viscoelasticity. IMA J Appl Math 81:522–537. doi: 10.1093/imamat/hxw031

Saramito P (2009) A new elastoviscoplastic model based on the Herschel-Bulkley viscoplastic model. J Nonnewton Fluid Mech 158:154–161.

Saramito P, Wachs A (2017) Progress in numerical simulation of yield stress fluid flows.

Swan JW, Zia RN, Brady JF (2014) Large amplitude oscillatory microrheology. J Rheol (N Y N Y) 58:1. doi: 10.1122/1.4826939

Thurston GB, Pope GA (1981) Shear Rate Dependence of the Viscoelasticity of Polymer-Solutions.2. Xanthan Gum. J Nonnewton Fluid Mech 9:69–78.

Tracey EM, Smith PA, Morrey E V (1996) Rheology of concentrated, heterogeneous slurries containing > 1M electrolyte - a case study in nuclear waste suspensions. J Nucl Mater 230:19–35. doi: 10.1016/0022-3115(96)00025-6

Wagner MH, Rolón-Garrido VH, Hyun K, Wilhelm M (2011) Analysis of medium amplitude oscillatory shear data of entangled linear and model comb polymers. J Rheol (N Y N Y) 55:495. doi: 10.1122/1.3553031

Weber E, Moyers-gonzález M, Burghelea TI (2012) Thermorheological properties of a Carbopol gel under shear. J

Nonnewton Fluid Mech 183–184:14–24. doi: 10.1016/j.jnnfm.2012.07.005

Zhou Y, Schroeder CM (2016) Transient and Average Unsteady Dynamics of Single Polymers in Large-Amplitude Oscillatory Extension. Macromolecules 49:8018–8030. doi: 10.1021/acs.macromol.6b01606